Adaptability of the ocean and earth tidal models based on global observations of the superconducting gravimeters

SUN Heping[1], Ducarme Bernard[2], XU Houze[1], Vandercoilden Leslie[2], XU Jianqiao[1] & ZHOU Jiangcun[1]

1. Key Laboratory of Geodynamic Geodesy, Institute of Geodesy and Geophysics, Chinese Academy of Sciences, Wuhan 430077, China;
2. Royal Observatory of Belgium, 3av. Circulaire, B-1180, Brussels, Belgium

Correspondence should be addressed to Sun Heping (email: heping@asch.whigg.ac.cn)

Received March 1, 2004; revised November 2, 2004

Abstract The adaptability of recent ocean tidal models and Earth tidal models is investigated comprehensively by means of 22 high precision tidal gravity observation series at 20 stations of the Global Geodynamics Project. Careful preprocessing of the original observations was carried out using international standard algorithms and the tidal gravity parameters were computed. The gravity load vectors of 8 main constituents are obtained based on loading computation theory and various global ocean models. The loading corrections of 14 secondary constituents are obtained based on a two-dimensional interpolation technique. Considering different characteristics of the wave amplitude, a method of "non-identical weighted mean" is developed for computing the averaged observed residual and remaining residual vectors at each station. The efficiency of the loading correction and the discrepancy between corrected amplitude factors and theoretical ones are analyzed. Meanwhile the calibration problem of the instruments is also discussed. After loading correction, the averaged tidal gravity parameters for all stations are obtained. The results show that the discrepancies between the global mean amplitude factors and theoretical values are less than 0.3%, the largest calibration error of the instruments is less than 0.5%. On the other hand, there are indications that the slight phase advance of K_1 with respect to O_1 in Mathews' theory could be verified by ground based tidal gravity observations.

Keywords: superconducting gravimeters, Global Geodynamics Project, determination of the tidal gravity parameters, verification of the global ocean and Earth tidal models.

DOI: 10.1360/04yd0071

As the gravity field is the most primary and direct physical quantity reflecting the density variation of the Earth's interior and its geodynamic properties under various environmental changes and as the knowledge of the fine structure of the Earth's interior and its geodynamics has a strong impact on space research, gravity observations become more and more important in Earth sciences. Therefore based on a global network of superconducting gravimeters (SGs), the Global Geodynamic Project (GGP) was launched in July 1997 inside the group for Study of the Earth's Deep Interior (SEDI) of the International Union of Geodesy and

Geophysics[1]. SGs made by the GWR company in USA are installed at all stations. Identical central sensors are equipped with similar data acquisition systems and filters. The different sampling rates are decimated to one minute intervals. Standard data processing and analyzing methods are recommended by the GGP group in order to obtain the tidal parameters at different bands of the Earth tides and to reduce the influence of various external perturbations on the records. In this study we consider 19 GGP stations, including 3 dual-sphere SGs and 16 single-sphere SGs. With its extremely wide dynamical linear measuring range, accuracy (10^{-10}ms^{-2}), small drift and long-term high stability (10^{-8} ms^{-2}/a), the superconducting gravimeter (SG) is the best tidal gravimeter. It gives us the opportunity of capturing the tiny signals induced by the geodynamical phenomena in the Earth's interior[2,3].

In recent years, much effective research works are contributed to theoretical tidal modeling and tidal gravity parameters determination by our colleagues. The tight relations between the tidal generating potential (precision 10^{-11}ms^{-2}), celestial mechanics and Earth's deformation have been well established[4–6]. However, the inversion studies of the ocean tidal models and the verification of the tidal gravity models based on global tidal gravity observations with SGs are just at the beginning, especially using global data. The published results are either based on single station and single ocean tide model or based on spring gravimeters[7–11]. Therefore it is necessary to make a general assessment on the various ocean tidal and Earth tidal models by utilizing the global SG observations, in order to better constrain the Earth's interior structure and its geodynamical parameters[12–14].

1 Processing of the SG observations

Under the framework of governmental scientific cooperation between China and Belgium, the effective cooperative researches among the Institute of Geodesy and Geophysics, Chinese Academy of Sciences, the Royal Observatory of Belgium (ROB), the GGP Data Center are developed. The data gathered in recent years by international data exchange are processed comprehensively in order to understand deeply the global ocean tidal and Earth tidal models by using high precision gravity techniques. In data processing, the detailed preprocessing of the original observations is carried out first by using a technique with quick, flexible, direct and effective man-machine interaction[15], based on a remove-restore technique. The wrong signals compounded in the raw series such as peaks, steps and so on..., are eliminated. The relatively short interruptions in the records due to the power-cuts and earthquakes are interpolated in terms of a synthetic tidal gravity modeling. The minute records are transformed to hourly values by the same filtering process applied to all the series at various stations. Considering that the difference of the data from high and low spheres is very small for the dual-sphere SGs, the stacking technique for both high and low series is applied. To carry out the pressure correction, the atmospheric gravity admittance is obtained by using a regression technique between tidal gravity residuals and station air pressure. The observational equations are constructed based on the hourly series and the tidal gravity parameters (including the amplitude factors and phase lags and their error estimation) are determined for various tidal groups using the ETERNA package[16]. Considering the high quality of the data recorded with an Askania spring gravimeter and its location at station Pecny in central Europe, this series of observation is included as background data in the present work[17]. So there are finally 22 series at 20 stations (30854 days, about 84.5 years). In order to accurately determine the dynamical effect of Earth's liquid core[18], the tidal constituents including those secondary ones near the resonance frequency are separated precisely from long series of records. Therefore the tidal parameters of 13 diurnal (D) waves (σ_1, Q_1, ρ_1, O_1, NO_1, π_1, P_1, K_1, ψ_1, φ_1, θ_1, J_1, OO_1) and of 9 semi-diurnal (SD) waves ($2N_2$, μ_2, N_2, ν_2, M_2, L_2, T_2, S_2, K_2) are finally determined. The later research shows that the accurate separation of tidal waves is highly beneficial to the determination of the resonance parameters of the Earth's liquid core. However, we will not provide in detail how to determine the parameters of the dynamical effect due to the limited volume of this article.

Table 1 gives the basic information of the GGP stations including coordinates, instrument model, data length, standard deviation of tidal parameters and admittance of atmospheric gravity respectively. The standard deviation reflects the quality of tidal parameters determination and the station background noise level. Smaller standard deviations mean highly accurate observations. Table 1 indicates low standard deviations up to (or less than) one nms^{-2} for the new style CT and CD model SGs and large standard deviation comparatively for the earlier T model SGs except for the one at Potsdam station. It shows that the new SG models provide higher quality data than the old ones. At Pecny station, a standard deviation at the nms^{-2} level is a proof for the quality of the observations. For most of the stations, the admittance of the atmospheric gravity is close to -3.0 nms^{-2}/hPa while at Matsushiro, Syowa and Pecny stations, the coefficient is a little bit larger and a little bit smaller at Sutherland station. These phenomena reflect the various pressure variation patterns in different areas. It may relate also to the station background noise. Not taking into account these 4 series, the global mean atmospheric gravity admittance is -3.36 ± 0.04 nms^{-2}/hPa, which approaches to the theoretical value (-3.60 nms^{-2}/hPa) computed with an atmospheric model under hypothesis of the hydrostatic equilibrium[19]. After excluding the tidal gravity signals, the station background noises is at the order of nms^{-2} in both temporal and frequency domains. As an example, Fig. 1 gives the characteristics of the gravity residuals in time and frequency domains at Wuhan station.

In order to assess the temporal stability of tidal parameters, the harmonic analysis is carried out separately to the SG observations at various stations by using unique technique. The long series records at Brussels, Strasbourg and Cantley stations are divided into several sections of two-year length, the stacking method is used for dual-sphere SG records while the individuals are processed respectively. The numerical results show that the discrepancy of amplitude factors for 8 main constituents when using the data in different time spans and instruments is less than 0.1%. It

Table 1 Basic station information, data length, standard deviation of tidal parameters and atmospheric gravity admittance

	No.	Station name	Lat/(°)	Lon/(°)	Instu.	*DL*/d	SD/nm·s^{-2}	ADD (nm·s^{-2}/hPa)
1	BE0200	Brussels/Belgium	50.7986	4.3581	T003	6,660	1.743	−3.467±0.005
2	MB0243	Membach/Belgium	50.6093	6.0066	CT21	1,728	1.007	−3.286±0.006
3	ST0306-1	Strasbourg/France	48.6223	7.680	T005	3,272	2.265	−3.128±0.010
4	ST0306-2	Strasbourg/ France	48.6223	7.680	CT26	817	0.797	−3.394±0.007
5	BR0515	Brasimone/Italy	44.1235	11.1183	T015	1,098	2.576	−3.053±0.036
6	VI0698	Vienna/Austria	48.2493	16.3579	CT25	729	0.662	−3.467±0.007
7	WE0731-1	Wetzell/German	49.1458	12.8794	T103	726	2.639	−3.374±0.031
8	WE0731-2	Wetzell/German	49.1458	12.8794	CD29	2x291	0.667	−3.340±0.009
9	PO0765	Potsdam/German	52.3809	13.0682	T018	2,250	0.855	−3.313±0.004
10	MO0770	Moxa/German	50.6450	11.6160	CD34	2x580	0.590	−3.320±0.005
11	ME0892	Metsahovi/Finland	60.2172	24.3958	T020	1614	1.299	−3.636±0.007
12	PC0930	Pecny/Czech	49.9200	14.780	ASK228	412	0.887	−4.894±0.013
13	WU2647	Wuhan/China	30.5139	114.4898	CT32	985	0.750	−3.237±0.010
14	KY2823	Kyoto/Japan	35.0278	135.7858	T009	686	3.323	−3.183±0.038
15	MA2834	Matsushiro/Japan	36.5430	138.2070	T011	880	1.163	−4.471±0.010
16	ES2849	Esashi/Japan	39.1511	141.3318	T007	875	1.286	−3.549±0.011
17	SU3806	Sutherland/South Africa	−32.3814	20.8109	CD37	(491+304)	0.689	−2.657±0.013
18	BA4100	Bandung/Indonesia	−6.8964	107.6317	T008	420	7.450	−3.524±0.243
19	CB4204	Canberra/Australia	−35.3206	149.0077	CT31	890	0.776	−3.392±0.010
20	BO6085	Boulder/U. S. A	40.1308	254.7672	CT24	1,401	0.997	−3.518±0.007
21	CA6824	Cantley/Canada	45.5850	284.1929	T012	2,386	1.443	−3.293±0.006
22	SY9960	Syowa/Antarctic	−69.0070	39.5950	T016	548	1.103	−4.115±0.009

T, The earlier SG; CT, new style SG; CD, dual-sphere SG; ASK, Askania spring gravimeter.

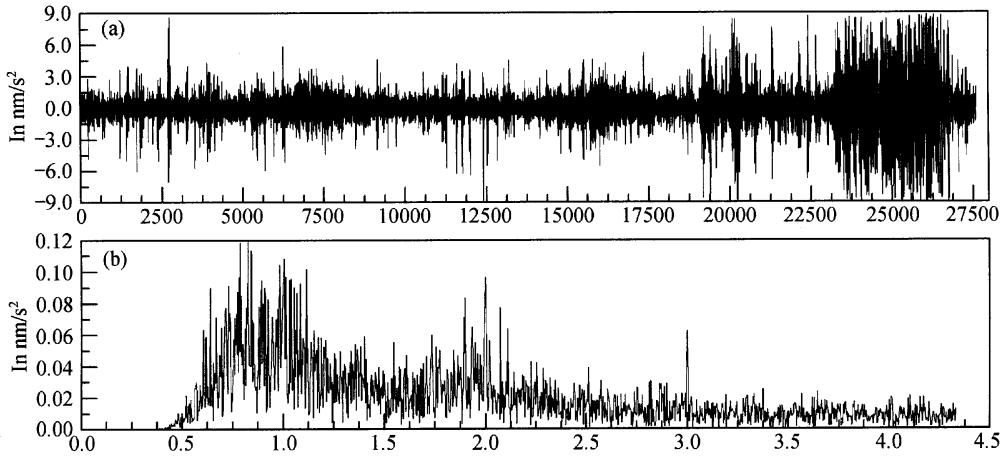

Fig. 1. Characters of the observed gravity residuals in time (a) and frequency (b) domains at Wuhan station (2000-03-31 09:00—2003-06-01 15:00).

confirms the excellent stability of the SG's observations. A relatively large discrepancy between T103 and CD29 at Wettzell station is due to a calibration problem[11]. The discrepancy of the amplitude factors between the new CT26 and the earlier T005 SG at Strasbourg station is 0.15% and the phase lags agree within 0.5°. These discrepancies remain inside the internal analysis error range.

2 Description of the tidal gravity and ocean tides models

The theoretical tidal gravity values constructed in recent years are based on given Earth models. Under the hypothesis of non-hydrostatic equilibrium, considering the Earth's rotation, the anisotropy and the inelasticity of the mantle, frequency dependent Love numbers are obtained by solving a group of the Earth's motion equations. The tidal gravity parameters are then obtained by combination of these Love numbers. The non-hydrostatic flattening of the mantle-core boundary is taken into account to determine precisely the parameters of the Earth's free core nutation. The determination of the Q factor of this resonance is important for studying mantle medium's damping. We shall refer hereafter to one of the most recent models[5] as DDW tidal gravity model. From a Q values model obtained with seismic observations, Mathews et al.[6] studied also the problem of the mantle inelasticity in tidal bands. He pointed out that the Q value is a frequency dependent power function with order of α. Using Q values at the reference periods of 1200s and 300s, the influence of the different power functions on Love numbers were obtained[6]. Using a Q value model for the reference period of 1s and $\alpha = 0.15$, Baker et al.[9] concluded that the tidal gravity model in central Europe is slightly bigger than the normal one. The effect of lateral inhomogeneity on the theoretical model was studied on the basis of a model of lateral asymmetry of degree 8 and order 8 obtained by seismic tomography. And the result show that the largest effect was only at the order of 10^{-11} ms^{-2}, due to the large difference between seismic frequencies and tidal ones[20].

The earlier ocean tide models are obtained by solving the Laplace tidal equations with considering the sea bottom friction, auto-gravitation attraction of sea water and loading deformation of the sea floor. However, there exist relatively large errors in these tidal models due to the complex dissipation effects resulting from sea bottom friction and to the low resolution of the grid. Schwiderski constructed the relatively accurate ocean tide models (SCW80) by the method of hydrodynamic interpolation introducing tide gauge data on coast lines and islands. It provided us for the first time with the relatively complete and basic ocean tidal model for loading correction in geodesy and geophysics[21]. Recently with the rapid development of

the finite element method and space technology, it became possible to correct effectively the errors over the shallow and deep sea areas. Using the Topex/Poseidon (T/P) satellite altimeter data, a series of new ocean tidal models have been developed[22]. Adopting the response method, Eanes et al. in University of Texas constructed the CSR3.0 models. Later on the updated CSR4.0 models are obtained with more T/P data and coast line tide gauge data[23]. Le Provost et al. constructed the FES952 ocean tide model. However, due to the orbital resolution (2.83°) of the altimeter, it is difficult to separate accurately tides over shallow sea[24]. Based on the T/P data and hydrodynamic equations, the new TPXO2 ocean models are constructed by Egbert et al.[25]. Using T/P data with an orbital resolution of 0.5° to improve shallow sea part and considering the tide gauge data on coastlines and islands in Japan and East Asia, the ORI96 models are constructed by Matsumoto et al. at the Institute of Oceanography, Kyoto University[26]. Melchior et al. studied the zero point pattern and characters of the cotidal lines by using ground based tidal gravity observations along the world. They compared tidal gravity observations with the results of loading computations on a global scale[7]. The statistic analysis of the characteristics of the recent ocean tide models show that the models obtained with the T/P data and by a finite element technique have high resolution and wide cover (especially over pole area) and that the determined precision of the residual amplitudes is higher than other models. For example, the residual amplitude of M_2 wave is reduced from 0.73 cm (SCW80) to 0.04 cm (FES952) and to 0.02 cm (CSR3.0).

3 Ocean loading correction of the observed tidal gravity residuals

The effect of the ocean loading on gravity field depends on the variation of the characteristics of the Earth's crust and upper mantle. The influence of the structural discrepancies of the ocean bottom and of the Earth's crust on gravity loading is much larger than their effects on body tides. The displacement response due to the ocean loading on various layers of sediments is much more sensitive to their constitution than their response to the body tides. Therefore, the computation of tidal gravity loading is much more complex than that of the body tide[27]. In order to compare the influence of the loading corrections based on various ocean models on the results of the tidal gravity analysis, the effect of the ocean tides on gravity observations is calculated with the SCW80, CSR3.0, FES952, TPXO2, CSR40 and ORI96 global ocean tidal models[14,28], using the integrated Green's functions developed by Agnew. As an example, Fig. 2 gives the amplitudes of the gravity loading vectors for 4 main constituents at Wuhan station. It is found that the loading amplitude reaches 6.0 nms^{-2} for the main waves (O_1, K_1 and M_2), and 3.0 nms^{-2} for the S2 wave. In general, at other stations, they are generally lower than 10.0 nms^{-2}. But the load effects in SD band are quite prominent at Sutherland station. The load amplitude of M_2 wave reaches the level of 58.0 nms^{-2} for instance. The present research shows that accurate correction can eliminate effectively the loading signals from tidal gravity observations.

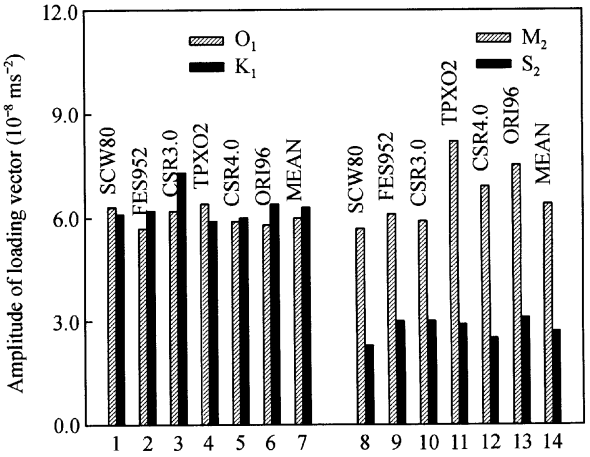

Fig. 2. Gravity loading amplitudes for 4 main constituents at Wuhan station.

As the ocean tides and Earth's gravity tidal signals are resulting from the same generating forces of the celestial bodies such as the sun, the moon and others, they have identical frequencies. Therefore the signals of the ocean tides and Earth tides are coupled together but in a quite complex way. However, there exist certain proportionality relations for both amplitudes, and also there exists a relation between the change in

phases and the distribution of the frequency. Frequently, the digital oceanic models provide us the amplitudes and phases of main constituents. So in order to get the value of the loading correction for those secondary constituents, especially the waves near the frequency of the nearly diurnal free wobble of the Earth's liquid core, it is necessary for us to carry out an interpolation in a complex plane. The amplitudes of the theoretical gravity tides are used to normalize those of the loading tides, taking into account the resonance effect of the Earth's liquid core. This effect is eliminated in the first step of calculation before the interpolation. After getting the real and imaginary parts of the loading amplitudes for these secondary constituents, the removed resonance signal is recovered. With 6 ocean models, the loading vectors of 14 secondary constituents are calculated (σ_1, ρ_1, NO_1, π_1, ψ_1, φ_1, θ_1, J_1, OO_1, $2N_2$, μ_2, ν_2, L_2 and T_2). These results agree with those obtained from the FES952 models for the same secondary constituents. It means that the loading vectors obtained using our interpolation technique correspond well with those calculated directly from the ocean models, it shows also that the interpolation technique is effective

As we are interested by the influence of the global ocean loading, it is necessary for us to assess objectively the efficiency of ocean loading correction. For any constituent, if the observed tidal amplitude vector is expressed as $\boldsymbol{A}(A,\alpha)$, and the theoretical value is $\boldsymbol{R}(R,0)$, we can define the observed residual vector as $\boldsymbol{B}(B,\beta)$ (Fig. 3). Then the relation among them will be $\boldsymbol{B}(B,\beta)=\boldsymbol{A}(A,\alpha)-\boldsymbol{R}(R,0)$. The relation among the final residual vector $\boldsymbol{X}(X,\chi)$, observed residual vector $\boldsymbol{B}(B,\beta)$, and computed ocean loading vector $\boldsymbol{L}(L,\lambda)$ will be given as $\boldsymbol{X}(X,\chi)=\boldsymbol{B}(B,\beta)-\boldsymbol{L}(L,\lambda)$.

After computation of the loading vectors, the loading correction of the tidal gravity observations can then be carried out. Using the SG data at Wuhan international tidal gravity reference station, Sun et al. studied the efficiency of the loading correction[8]. The

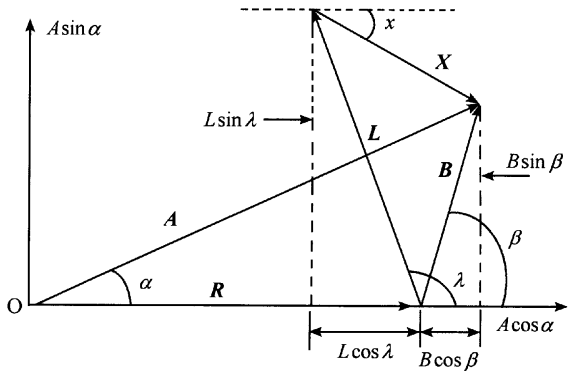

Fig. 3. Relationship among observed tidal gravity amplitude vector $\boldsymbol{A}(A,\alpha)$, theoretical model $\boldsymbol{R}(R,0)$, computed oceanic tidal loading vector $\boldsymbol{L}(L,\lambda)$, tidal residue vector $\boldsymbol{B}(B,\beta)$ and final residual vector $\boldsymbol{X}(X,\chi)$.

results showed that the corrected gravity residuals are reduced significantly, compared to the theoretical models, the discrepancy of the mean amplitude factors for 8 main waves are reduced from 1.38% to 0.13% (CSR3.0) and 0.26% (FES952) for instance.

In practice, it is quite difficult to evaluate effectively the suitability of ocean models and the efficiency of loading correction by simply averaging technique. In order to obtain the evaluation of the observed residuals and remaining residuals of the tidal gravity observations, the method of "non-identical weighted mean" is introduced in both D and SD bands. It is based on the consideration of the different amplitudes and error characteristics of the various tidal constituents.

In order to assess entirely the efficiency of the oceanic loading correction, the observed residual vectors and remaining residual vectors are normalized by the theoretical amplitude of the corresponding tidal wave ($\boldsymbol{B}/R$ and $\boldsymbol{X}/R$) in a first step. Then the non-identical weighted mean of the main constituents is processed, with the weights being proportional to the amplitudes of the constituents. Therefore the mean observed residual vectors ($M_D(\boldsymbol{B})$, $M_{SD}(\boldsymbol{B})$) and mean remaining residual vectors ($M_D(\boldsymbol{X})$, $M_{SD}(\boldsymbol{X})$) in D and SD bands are then computed by the following formula:

$$M_D(i)=[2\times A(O_1)+A(P_1)+3\times A(K_1)]/6,$$
$$M_{SD}(i)=[2\times A(M_2)+A(S_2)]/3, \quad (1)$$

where $i=1$ for the observed residual vector $\boldsymbol{B}$ and $i=2$ for the remaining residual vector $\boldsymbol{X}$. A is the amplitude of the normalized residual vector $\boldsymbol{B}$ or the remaining residual vector $\boldsymbol{X}$. The quantity in parenthesis is the name of corresponding waves. Therefore the efficiency of the loading correction E_D (in D band) and E_{SD} (in SD band) can be calculated as

$$E_D=(M_D(\boldsymbol{B})-M_D(\boldsymbol{X}))/M_D(\boldsymbol{B}),$$
$$E_{SD}=(M_{SD}(\boldsymbol{B})-M_{SD}(\boldsymbol{X}))/M_{SD}(\boldsymbol{B}). \quad (2)$$

As an example, Fig. 4 gives the efficiency of the loading correction for the main constituents at Wuhan station. It shows that the efficiency reaches 80% (or more). For some stations in Europe, such efficiency can reach more than 90%. Table 2 gives the mean observed residual vectors $M_D(\vec{B})$ and $M_{SD}(\vec{B})$, mean remaining residual vectors $M_D(\boldsymbol{X})$ and $M_{SD}(\boldsymbol{X})$ and the mean efficiencies of the loading correction E_{SD} and E_D in D and SD bands for 21 SG and 1 spring gravimeter at 20 stations. In this table, the residuals are scaled in function of the theoretical amplitude for corresponding waves and thus expressed in percentage.

From the table, it is found that the observed residual vectors at most of stations are reduced significantly in D band. The efficiency at 9 stations is more than 80%, the best one arrives at 97.2% (Bandung). While for some stations in West Europe, the correction efficiency is relatively low, it is less than 40% for 4 stations located in West Europe (Brussels, Brasimone, Wetzell and Metsahovi). This fact is related to the small amplitudes of the D waves over the North Atlantic and the associated weak loading effect (lower than 0.5%). The numerical results also show that the correction efficiency is not good in SD band when the SCW80 and TPX02 models are used[11]. Therefore

Table 2 Mean efficiency of the ocean loading correction averaged with different ocean models at various stations

Station	Mean for 6 ocean tide model in diurnal band					Mean for 4 ocean tide model in semidiurnal band *				
	$M_D(\boldsymbol{B})$		$M_D(\boldsymbol{X})$		E_D	$M_{SD}(\boldsymbol{B})$		$M_{SD}(\boldsymbol{X})$		E_{SD}
	B (%)	β/(°)	X (%)	χ/(°)	%	B (%)	β/(°)	X (%)	χ/(°)	%
BE0200	0.36	93.94	0.39	−28.54	−7.6	5.10	60.44	0.50	−70.84	90.3
MB0243	0.42	103.19	0.03	−55.20	91.9	4.73	56.15	0.15	−103.95	96.9
ST0306	0.46	127.69	0.16	−169.13	66.3	4.13	55.51	0.23	−120.24	94.4
ST0306	0.31	111.64	0.11	−79.75	65.2	4.14	53.15	0.29	−84.88	92.9
BR0515	0.59	146.84	0.36	−157.10	39.1	2.25	47.26	0.56	−118.43	75.1
VI0698	0.43	139.07	0.14	−168.50	66.9	2.37	40.45	0.33	−120.14	86.1
WE0731	0.67	158.51	0.48	−169.57	28.5	2.68	51.83	0.59	−156.66	78.2
WE0731	0.58	108.94	0.22	100.03	62.8	3.40	52.72	0.39	109.45	88.5
PO0765	0.37	95.33	0.08	22.72	78.7	3.25	43.80	0.07	−57.85	97.7
MO0770	0.41	111.83	0.03	124.34	91.9	3.34	48.34	0.19	−156.35	94.4
ME0892	0.43	33.50	0.54	7.79	−26.0	2.01	30.91	0.27	−31.26	86.6
PC0930	0.29	98.74	0.11	−14.71	65.2	2.62	38.76	0.42	−105.12	84.1
WU2647	2.16	−23.39	0.38	6.52	82.5	1.38	−27.53	0.29	−11.77	79.3
KY2823	5.27	2.85	0.24	57.55	95.5	4.12	1.88	0.12	104.35	97.0
MA2834	4.77	4.91	0.19	−144.22	96.0	3.25	12.55	0.28	−120.98	91.3
ES2849	6.67	11.98	0.52	−12.96	92.2	4.63	33.69	0.63	−11.005	86.3
SU3806	0.75	−57.46	0.24	−74.44	68.5	10.02	86.57	0.15	−29.47	98.5
BA4100	20.88	93.94	0.57	−174.12	97.2	2.42	−37.40	0.61	102.27	74.6
CB4204	1.85	−61.53	0.40	−2.57	78.5	4.64	−71.43	0.33	−84.23	93.0
BO6085	3.00	60.87	0.22	49.00	92.6	0.48	77.14	0.27	−112.09	43.4
CA6824	1.59	40.92	0.49	−8.42	69.2	3.84	−24.01	0.62	−107.37	83.7
SY9960	8.23	5.95	1.22	−18.09	85.2	27.08	0.97	6.36	5.37	76.5

* CSR30, FES952, CSR40 and ORI966.

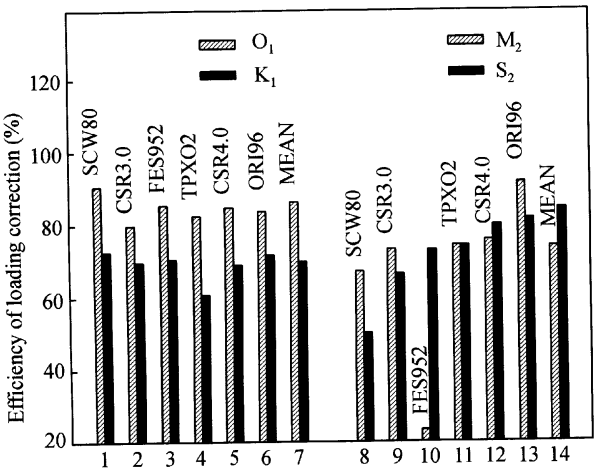

Fig. 4. Efficiency of the loading correction for 4 main constituents at Wuhan station.

only the results obtained with 4 ocean models (CSR30, FES952, CSR40 and ORI966) are averaged in Table 2. Generally speaking, except for the results from Boulder station, the efficiency of the loading correction is obvious, 16 series reach 80% or more and the best one climbs to 97.7% at Potsdam station.

On the other hand, for the best mean results at all stations in D band, the correction efficiency is 88.8% (SCW80), 93.1% (CSR3.0), 96.3% (FES952), 95.9% (TPXO2), 94.7% (CSR4.0), 93.0% (ORI96) respectively. In SD band the corresponding results are 82.5% (SCW80), 93.6% (CSR3.0), 94.6% (FES952), 77.6% (TPXO2), 88.5% (CSR4.0), 94.9% (ORI96). It shows definitely that the main part of the tidal gravity residuals is due to ocean tides. The smaller the remaining residuals are, the more complete, better and more effective the loading correction is.

Meanwhile, one can suspect a calibration error if the phase of the final residue X is near 0° or 180°. Based on the phase characteristics of remaining residuals, the calibration problem of the instruments may be studied by averaging the remaining residual vectors after loading correction with various ocean models. In D band, the residual amplitudes of 12 series in Europe are less than 0.5%, and they are 2%—3% in North America. However, at Esashi and Kyoto stations in Asia, they reach 5% and 20% in Bandung. In SD band, there exists a tendency from west to east for the residual amplitudes of 12 series over Europe (from 5% to 2.5%). The loading correction is less efficient at Syowa and Bandung stations. It is due to the stations' geographic location. The former is located on the Antarctic coastline where the ocean tide model is not complete and the latter is located in Indonesia islands where the ocean tide pattern is much more complicated. For Boulder station in North America, the efficiency of loading correction is only 43.4% in SD band. It is related to the small amplitude of the ocean tide loading, with Boulder being a continental station. The analysis shows that amplitudes of remaining residuals at Brasimone, Brussels and Wettzell stations reach to 0.5%. The similar situation happens at Kyoto, Esashi and Cantley stations. Therefore a 0.5% instrumental calibration error can be suspected in some of those stations. Unfortunately, in the SD band, it is not evident that one ocean model is better than another just in terms of amplitudes of the remaining residuals as some models can be better in some regions and worse in other ones.

4 Tidal gravity parameters corrected of the ocean loading

Tidal analysis was performed using the standard ETERNA3.4 software recommended by the International Earth Tides Commission (IETC). First the hourly data are band pass filtered to eliminate the instrumental drift. Then the various waves in D, SD and ter-diurnal (TD) bands are separated considering the properties of the angle frequency of the various waves and those of the odd and even band pass filters. The tidal gravity parameters, i.e. the amplitude factors and phase lags for various tidal waves, are obtained with their error estimations by solving observational equations with a classical least-square technique[16]. By removing synthetic tidal gravity from observational signals, the changes in tidal gravity residuals in temporal domain can be obtained. In the data analysis, we used the tides generating potential development given by Tamura of National Observatory of Japan[29].

The loading corrections of the tidal gravity observations are carried out for various components with different ocean tides models. As an example, Fig. 5

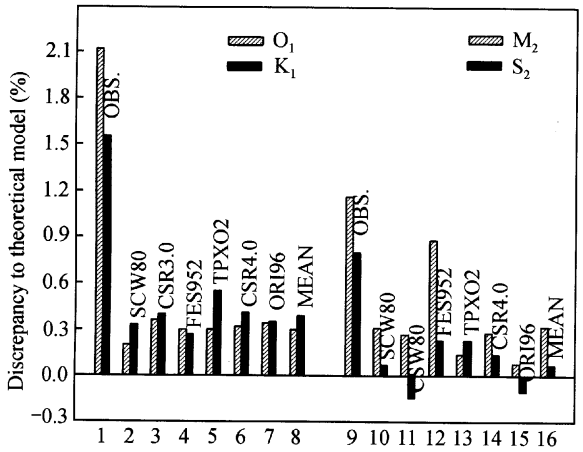

Fig. 5. Discrepancy of the amplitude factors before and after ocean loading correction compared to the theoretical model for 4 main waves at station Wuhan.

gives the discrepancies of the amplitude factors for 4 constituents compared to the theoretical model before and after ocean loading correction. The comparison shows that after loading correction, the amplitude factors are much closer to the theoretical values. At Wuhan station, the discrepancies of the main waves O_1, K_1, M_2 and S_2, are reduced from (2.13, 1.56, 1.16 and 0.84%) before loading correction to (0.32, 0.40, 0.33 and 0.11%) after correction respectively. Whereas poorly modeled loading effects over some areas with complicated coastline and regional tides are still leaving large discrepancies of the tidal parameters. For minor constituents such as ψ_1 and φ_1 the signal to noise ratio is also very poor in some stations. In order to consider comprehensively the global parameters, triple standard deviation (3σ) criterion is used as a critical value for the elimination of anomalous results. Additionally, in SD band, the efficiencies of the loading correction obtained with the SCW80 and TPXO2 models are lower[11]. So the results from these two models have not been included when averaging the global tidal parameters.

Table 3 gives the comparison between the mean tidal parameters of all observation series after loading correction and the theoretical models (13 waves in D band and 9 waves in SD band). Among them, the mean results are computed in D band for 6 ocean tidal models and in SD band for 4 ocean models only. The numbers in brackets following the wave name in first column are the numbers of the observation series with SG. Some lower quality series were excluded for some waves, as at Syowa, Kyoto and Brasimone stations, according to the 3σ criterion. For instance, 21 series are given for K_1 and P_1 waves and only 16 series for ψ_1. K_1 and P_1 have the smallest standard deviations with an error of 0.3% on the amplitude factor and 0.08° on the phase differences.

Table 3 Comparison of the mean tidal gravity parameters after ocean loading correction for all stations with theoretical models

Constituent (*N*)	Diurnal band					Constituent (*N*)	Semidiurnal band			
	Tidal parameter/(°)		σ	DDW model	SXD2 model		Tidal parameter/(°)		σ	DDW model
σ_1(19)	1.1550	0.164	0.47	1.1542	1.15467	$2N_2$(13)	1.1623	−0.169	0.68	1.1619
Q_1(20)	1.1538	0.044	0.37	1.1543	1.15458	μ_2(19)	1.1609	−0.247	0.80	1.1619
ρ_1(17)	1.1545	0.017	0.35	1.1543	1.15457	N_2(18)	1.1613	−0.086	0.35	1.1619
O_1(20)	1.1544	0.010	0.32	1.1543	1.15440	ν_2(21)	1.1598	−0.045	0.50	1.1619
NO_1(19)	1.1553	−0.023	0.58	1.1539	1.15386	M_2(19)	1.1602	0.008	0.31	1.1619
π_1(17)	1.1510	−0.054	0.67	1.1507	1.15091	L_2(16)	1.1604	−0.313	1.14	1.1619
P_1(21)	1.1501	−0.039	0.29	1.1491	1.14949	T_2(15)	1.1616	−0.360	0.51	1.1619
K_1(21)	1.1362	0.025	0.31	1.1348	1.13664	S_2(19)	1.1603	−0.229	0.16	1.1619
ψ_1(16)	1.2630	0.073	1.36	1.2717	1.25993	K_2(20)	1.1634	−0.034	0.31	1.1619
φ_1(19)	1.1691	0.061	0.79	1.1706	1.16856					
θ_1(18)	1.1569	0.097	0.79	1.1571	1.15643					
J_1(19)	1.1557	0.014	0.52	1.1569	1.15622					
OO_1(18)	1.1513	0.300	0.75	1.1563	1.15557					

N, The number of series used, σ standard deviation of tidal analysis; DDW, Dehant-Defraign-Wahr's hydrostatic equilibrium theoretical Earth tidal model; SXD: Sunheping-Xujianqiao-Ducarme's experimental Earth tidal model considering the resonance of liquid core on the basis of SG observations.

For convenience, Table 3 also gives the DDW99 theoretical tidal model obtained under the hypothesis of non-hydrostatic equilibrium. In D band, the SXD2 experimental tidal model was built considering parameters of the liquid core resonance based on global SG observations[30]. It is found that the global mean amplitude factor of O_1 wave is reduced from 1.1614 (before loading correction) to 1.1544 (after loading correction). Compared to the DDW99's model, the discrepancy is reduced from 0.62% to 0.1%, showing the good agreement between observed amplitude factor and theoretical values. The discrepancy of K_1 wave is only at the order of 10^{-4} level. It is less than its standard deviation. For the secondary constituents near the resonant frequency of liquid core (ψ_1 and φ_1 waves), the precision of standard deviation improves significantly. For ψ_1 wave, the discrepancy between observed and theoretical values is just at the level of experimental error and the phase lag is tiny positive. It is found from Table 3 that the phase advance of K_1 with respect to O_1 predicted by Mathews is also verified[3]. However, the magnitude of this effect is in the error range of the phase lag[6]. In SD band, the amplitude factors of main constituents agree well with the theoretical model. The relative discrepancy is at the order of 0.2%. For secondary constituents such as $2N_2$, N_2 and T_2, the largest discrepancy is even at the level of 0.1%.

5 Conclusions

Based on the 22 tidal gravity observation series at 20 stations and the most recent ocean tide models, the adaptability of the various global ocean tides models and Earth tidal models is studied systematically. The tidal parameters, i.e. the amplitude factors, phase differences and corresponding error estimations, are obtained by preprocessing and analyzing the original SG observations of the GGP network. Using the technique of Agnew's integrated Green's function, the loading correction values of 8 main constituents (Q_1, O_1, P_1, K_1, N_2, M_2, S_2 and K_2) are calculated with 6 ocean tide models. The loading vectors of secondary constituents in D and SD domains are interpolated using a two-dimension plane interpolation technique, taking into account the resonance effect of the Earth's liquid core on the ocean tides. It is found that the loading correction for those waves at resonant frequency as ψ_1 and φ_1 is quite effective. In order to assess entirely the suitability of the ocean and Earth tidal models, a technique of "non-identical weighted mean" is proposed in D and SD domains respectively for the computation of the global mean observed residuals and remaining residuals. The efficiency of the loading correction is studied and the discrepancies of the amplitude factors before and after loading correction compared to theoretical models are obtained. It is found that the correction efficiency is lower with SCW80 models in D and SD bands while it is lower with TPXO2 models in SD band. After loading correction, the discrepancies of observed amplitude factors with respect to the theoretical models are reduced significantly. It is shown that the tidal parameters observed with SGs agree well with theoretical models of DDW99 and with the SXD2 experimental model for what concerns the influence of the nearly diurnal free wobble. The discrepancies between global mean amplitude factors and theoretical ones are less than 0.3%. The phase advance of K_1 with respect to O_1 predicted by Mathews' theoretical computation is eventually verified from tidal gravity observations, but further investigations are required. The low quality of the loading correction at some stations is due to the complicated characters of regional ocean tides and for coastal stations to the inadequate representation of local effects. Therefore, further studies will require more accurate ocean tide models. Additionally, considering the remaining residuals calibration errors up to 0.5% can be suspected in some stations.

Acknowledgements The authors would like to give their gratitude to Prof. Crossley, the chairman of the GGP group, St. Louis University in USA, and all station observers in the GGP network for their hard work in obtaining the high quality data. This work was supported jointly by the Knowledge Innovation Project (Grant No. KZCX3-SW-131) and the Hundred Talents Program, the Chinese Academy of Sciences, the National Natural Science Foundation of China (Grant No. 40374029) and the Key International Scientific Cooperation Project via the Ministry of Sciences and Technology of China (Grant No. 2002CB713904).

References

1. Crossley, D., Hinderer, J., Casula G. et al., Network of superconducting gravimeters benefits a number of disciplines, EOS, 1999, 80(11): 121,125−121,126.

2. Goodkind, J. M., The superconducting gravimeters principals of operation, current performance and future prospects 1990. In: Poitevin C ed. Proceedings of the workshop on non-tidal gravity changes. via Conseil de L'Europe Cahiers du Centre Européen de Géodynamique et de Séismologie, Luxembourg. 1991, 9: 81—90.
3. Sun, H. P, Xu, H. Z., Execution and prospect for the global geodynamics project cooperation, Advance in Earth Sciences (in Chinese), 1997, 12(2): 152—157.
4. Wahr, J. M., Sasao, T., A diurnal resonance in the ocean tide and in the Earth's load response due to the resonant free core nutation, Geoph. J. R. Astr. Soc., 1981, 64: 747—765.
5. Dehant, V., Defraigne, P., Wahr, J., Tides for a convective Earth, J. Geophys. Res., 1999, 104(B1): 1035—1058.
6. Mathews, P. M., Love numbers and gravimetric factor for diurnal tides, Proc., 14th Int. Symp. on Earth Tides, J. Geodetic Society of Japan, 2001, 47(1): 231—236.
7. Melchior, P., Francis, O., Comparison of recent ocean tide models using ground-based tidal gravity measurements, Marine Geodesy, 1996, 19: 291—330.
8. Sun, H. P., Xu, H. Z., Luo, S. C. et al., Study of the ocean models using tidal gravity obsetvations obtained with superconducting gravimeter, Acta Geodaetica et Cartographica Sinica (in Chinese), 1999, 28(2): 115—120.
9. Baker, T. F., Curtis, D. J., Dodson, A. H., A new test of Earth Tide models in Central Europe, Geophys. J. Int., 1996, 107: 1—11.
10. Ducarme, B., Sun, H. P., Tidal gravity results from GGP network in connection with tidal loading and Earth response, Proc. 14th Int. Symp. on Earth Tides, J. Geodetic Society of Japan, 2001, 47(1): 308—315.
11. Ducarme, B., Sun, H. P., Xu J. Q., New investigation of tidal gravity results from the GGP network, Bull. Inf. Marées Terrestres, 2002, 136: 10761—10775.
12. Sun, H. P., Takemoto, S., Hsu, H. T. et al., Precise tidal gravity recorded with superconducting gravimeters at stations Wuhan/China and Kyoto/Japan, J. Geodesy, 2001, 74: 720—729.
13. Sun, H. P., Hsu, H. T., Xu, J. Q. et al., Determination of the new tidal parameters obtained with a superconduction gravimeter at station Wuhan/China, J. Geodetic Society of Japan, 2001, 47(1): 347—352.
14. Sun, H. P., Zhou, J. C., Correction problem of the ocean loading signals on gravity measurements at fundamental stations in crust movement observation network in China, Advance in Earth Sciences, 2002, 17(1): 39—43.
15. Vauterin, P., Tsoft: graphical & interactive software for the analysis of Earth Tide data, Proc. 13th Symp. Earth Tides, Brussels, Observatoire Royal de Belgique, Série Géophysique, 1998, 481—486.
16. Wenzel, H. G., The nanogal software: data processing package ETERNA 3.3, Bull. Inf. Marées Terrestres, 1996, 124: 9425—9439.
17. Broz, J., Simon, Z., Zeman, A., Tidal station Pecny: Results of 20 years of observation with the gravimeters GS15 No 228. VUGTK, Proceedings of Research Work, 1996, 75—88.
18. Sun, H. P., Hsu, H. T., Jentzsch, G. et al., Tidal gravity observations obtained with superconducting gravimeter and its application to geodynamics at Wuhan/China, J. Geodynamics, 2002, 33(1-2): 187—198.
19. Sun, H. P., Static deformation and gravity changes at the Earth's surface due to the atmospheric pressure, Geophysical Series of Royal Observatory of Belgium, 1995, 1—280.
20. Kopaev, A., Kuznetsov, F., Modeled and observed anomalies of tidal gravity factors, Phys. And Chem. of the Earth, 2000, 25: 395—399.
21. Schwiderski, E. W., Ocean Tides I, Global ocean tidal equations, Marine Geodesy, 1980, 3: 161—217.
22. Shum, C. K., Andersen, O. B., Egbert, G. et al., Comparison of Newly Available Deep Ocean Tide Models by the TOPEX/POSEIDON Science Working Team, J. Geophys. Res., 1997, 102(C11): 25173—25194.
23. Eanes, R. J., Bettadpur, S. V., The CSR 3.0 Global Ocean Tide Model: Diurnal and Semi-diurnal Ocean Tides from TOPEX/POSEIDON Altimetry, CSR Technical Memorandum 95-06, Center for Space Research, The University of Texas at Austin, Austin, Texas, USA, 1995.
24. Le Provost, C., Genco, M. L., Lyard, F. et al., Spectroscopy of the ocean tides from a finite element hydrodynamic model, J. Geophysical Research, 1994, 99(C12): 24777—24797.
25. Egbert, G., Bennett, A., Foreman, M., TOPEX/Poseidon tides estimated using a global inverse model, J. Geophys. Res., 1994, 99(C12): 24821—24852.
26. Matsumoto, K., Ooe, M., Sato, T. et al., Ocean tides model obtained from TOPEX/POSEIDON altimeter data, J. Geophys. Res., 1995, 100: 25319—25330.
27. Sun, H. P., Comprehensive researches for the effect of the ocean loading on gravity observations in the Western Pacific Area, Bull. Inf. Marées Terrestres, 1992, 113: 8271—8292.
28. Agnew, D. C., A program for computing ocean-tide loading, J. Geophys. Res., 1997, 102(B3): 5109—5110.
29. Tamura, Y., A harmonic development of the tidal generating potential, Bull. Inf. Marees Terrestres, 1981, 64: 677—704.
30. Sun, H. P., Xu, J. Q., Ducarme, B., Experimental earth tidal models in cinsidering nearly diurnal free wobble of the earth's liquid core, Chinese Science Bulletin, 2003, 48(9): 935—940.